Sensors and Materials, Vol. 35, No. 2 (2023) 529–536
MYU Tokyo

S & M 3191

Thermostable Europium Polymer Crystalline Spherical Beads and Their Photophysical Properties

Takayuki Nakanishi,[1*] Jian Xu,[2] Naoto Hirosaki,[1] and Takashi Takeda[1]

[1]Research Center for Functional Materials, National Institute for Materials Science (NIMS),
1-1 Namiki, Tsukuba, Ibaraki 305-0044, Japan
[2]International Center for Young Scientists (ICYS), National Institute for Materials Science (NIMS),
1-1 Namiki, Tsukuba, Ibaraki 305-0044, Japan

(Received October 1, 2022; accepted January 5, 2023)

Keywords: coordination crystals, luminescence property, europium

Among the various luminescent material series, lanthanide coordination polymer crystals have attracted attention for their characteristic photophysical properties based on the arrangement of lanthanide ions and organic linker ligands. Here, we demonstrate the morphology controllability of the thermostable crystalline europium coordination polymer $[Eu(hfa)_3dpbp]_n$, [hfa: hexafluoro-acetylacetonate; dpbp: 4,4'-bis(diphenylphosphoryl) biphenyl] to realize transparent phosphors. The obtained spherical Eu^{3+}-coordination particles were characterized using X-ray diffraction, scanning electron microscopy, dynamic light scattering measurements, and thermogravimetric analysis. The knowledge obtained is expected to be widely used as a transparent material development technique for new lanthanide-based coordination phosphors.

1. Introduction

Luminescent lanthanide coordination polymer crystals (LCPCs) with thermal stability are novel candidate phosphors for transparent luminescence applications such as mini-LED displays,(1) security inks,(2) and wavelength convertors for solar cells.(3,4) Various types of characteristic luminescent lanthanide complex have been reported for next-generation optical applications.(5–8) We previously reported thermostable europium coordination polymer crystals composed of europium ions and organo-phosphine oxides (decomposition temperature > 308 °C).(9) Their tight packing structures using intermolecular interaction induced effective thermostability and a small nonradiative rate constant k_{nr} for strong luminescence. Europium coordination polymer crystals have a high emission quantum yield. Thermostable coordination polymers are promising candidates for practical optoelectronic devices. However, those of LCPCs with thermal stability form large crystals of 10 μm order and insoluble compounds in water and organic solvents. Insoluble microsize polymer crystals cause multiple light scattering in the UV–visible region, giving an opaque appearance to the optical material. In contrast, if nanoparticles of LCPCs were available, they could be useful materials for increasing the transmittance of luminescent materials.

*Corresponding author: e-mail: Takayuki.Nakanishi@nims.go.jp
https://doi.org/10.18494/SAM4150

ISSN 0914-4935
https://myukk.org/

In this study, we investigated in detail the material morphology resulting from dispersing insoluble LCPCs in organic solvents. The obtained Eu^{3+}-coordination samples were characterized using X-ray diffraction (XRD), scanning transmission electron microscopy (STEM), dynamic light scattering (DLS) measurements, and thermogravimetric analysis (TGA). Their photophysical properties were estimated using emission spectra, excitation spectra, and emission lifetimes. We successfully observed the crystalline spherical $[Eu(hfa)_3dpbp]_n$ polymer and discuss its formation mechanism.

2. Materials and Methods

2.1 Preparation of $[Eu(hfa)_3dpdp]_n$ coordination polymer crystal

See Ref. 9 for the detailed procedure for synthesizing conventional $[Eu(hfa)_3dpdp]_n$. Figure 1(a) shows the preparation scheme of $[Eu(hfa)_3dpbp]_n$ polymers. A solution of 4,4'-bis(diphenylphosphoryl) biphenyl (dpbp) (0.40 g, 0.72 mmol) in 15 mL of MeOH was added to a solution of $Eu(hfa)_3(H_2O)_2$ (0.58 g, 0.72 mmol) in 10 mL of MeOH. The solution was stirred at 60 °C for 8 h and then filtered. The synthesis conditions were the same as previously reported,[9] and insoluble crystals with a size of 10 μm order were obtained. A dissolution test of $[Eu(hfa)_3dpbp]_n$ was carried out [Fig. 1(b)]. This insoluble LCPC (100 mg) was stirred in 50 mL of MeOH at 60 °C for 30 min. When the powder was added to methanol and dispersed, it formed a white suspension (left two pictures). For the solutions that become clear after resting for 1 day (right two pictures), the precipitate (named Sample 1) was collected by filtration. In addition, the clear supernatant solution was centrifuged and then filtered through a nanomembrane filter. The obtained fine powder was named Sample 2.

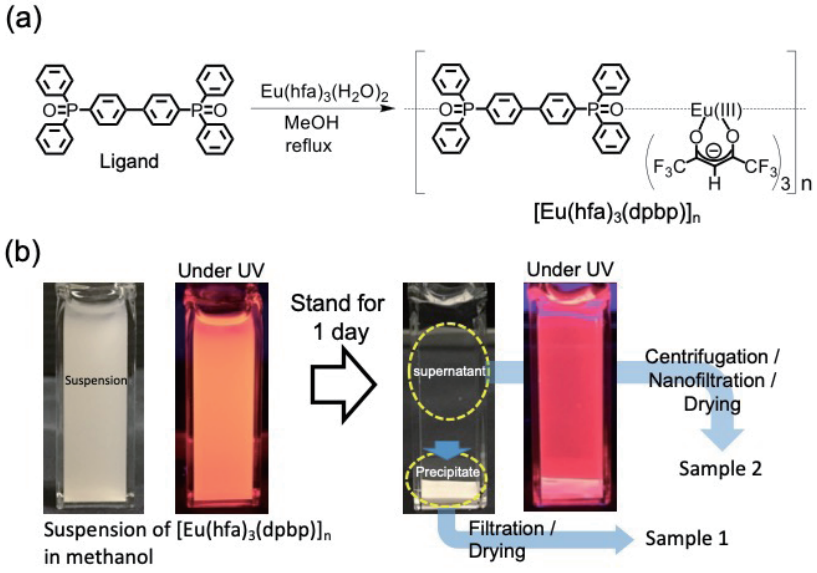

Fig. 1. (Color online) (a) Preparation scheme of $[Eu(hfa)_3dpbp]_n$ polymers. (b) Dissolution test of $[Eu(hfa)_3dpbp]_n$ for MeOH.

2.2 Apparatus

The luminescence properties of the samples were characterized on the basis of photoluminescence (PL) and PL excitation (PLE) spectra and lifetimes. The 4*f*–4*f* emission quantum yields (Φ_{Ln}) of the samples were estimated to calculate the radiative (k_r) and nonradiative (k_{nr}) rate constants. The crystal structures were measured by powder XRD (Smart Lab, Rigaku, Japan) utilizing nickel-filtered Cu Kα1 radiation (1.5406 Å). TGA was performed on a SEIKO EXSTAR 6000 system (TG-DTA 6300). The powder morphology was observed by SEM (JEOL, Japan). PLE and PL spectra were measured using a spectrofluorometer (FP-8650, JASCO, Japan) and calibrated using a standard halogen lamp. Decay curves were measured using a spectrometer (HORIBA Jobin Yvon, FluoroCube-NL 1000UHS, Japan) and a pulse laser diode (HORIBA Jobin Yvon, Delta Flex and 375 nm NonoLED).

3. Results and Discussion

3.1 Structural features and thermal stability of two types of $[Eu(hfa)_3dpdp]_n$ polymer

Figure 2 shows XRD patterns of the obtained $[Eu(hfa)_3dpbp]_n$ polymers: (a) Sample 1, (b) Sample 2, and (c) the calculated peak pattern of CIF data for $[Eu(hfa)_3dpbp]_n$ from our previous report.[9] The obtained diffraction patterns (a) and (b) are in good agreement with the single-crystal structure data (c), especially for the matching of the low-angle diffraction peaks around 7–11° {(200), (11-1), (111), (002)} derived from the heavy-metal periodic structure, indicating that the base structure is the $[Eu(hfa)_3dpdp]_n$-LCPC series. In addition, the diffraction pattern around 20° in Sample 2 is slightly disordered, suggesting that the short-range order around europium is different from that in the crystal of Sample 1.

To characterize the 3D fine structure, Fig. 3 shows FE-SEM images of (a) Sample 1 and (c) Sample 2 on carbon mesh TEM grids. Particles with a block-type shape and a size of around 10–30 μm were observed in Sample 1. In contrast, spherical particles were observed in Sample 2,

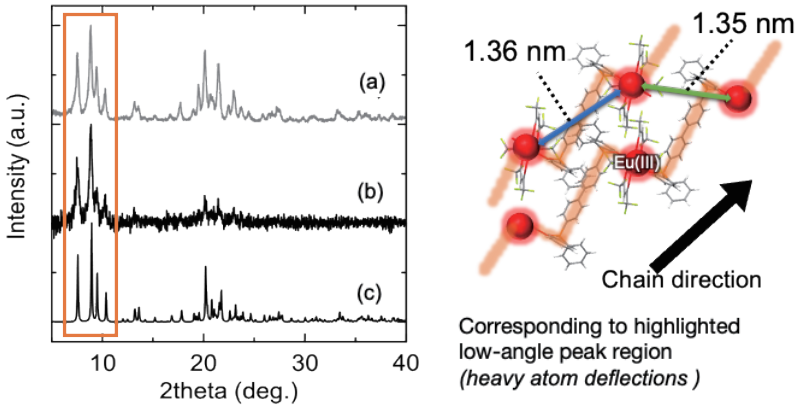

Fig. 2. (Color online) XRD patterns of $[Eu(hfa)_3dpbp]_n$: (a) Sample 1, (b) Sample 2, and (c) CIF data of $[Eu(hfa)_3dpbp]_n$.[9]

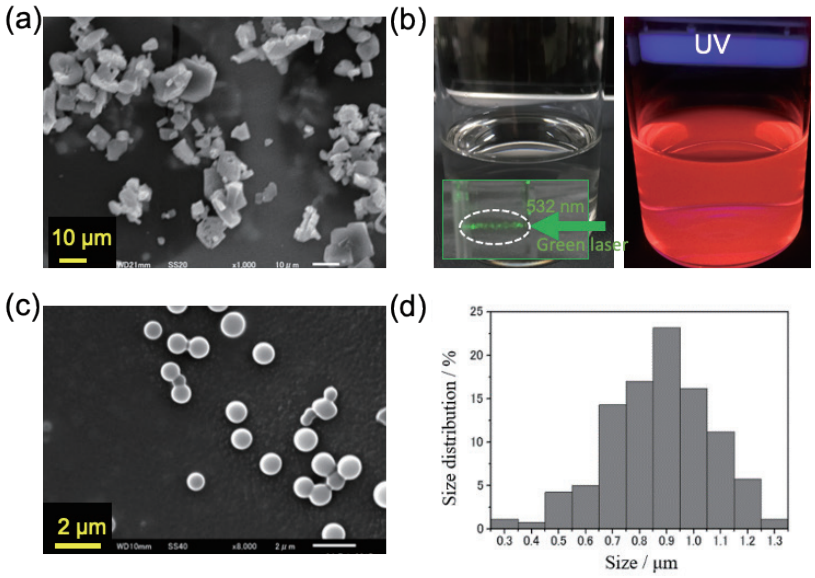

Fig. 3. (Color online) (a) FE-SEM image of Sample 1 on carbon TEM grid. (b) Appearance of supernatant of methanol dispersion liquid. (c) FE-SEM image of Sample 2 on carbon TEM grid. (d) Size distribution of Sample 2 in MeOH obtained by DLS measurement.

and their size was visually estimated to be around 600–800 nm. In addition, when the clear supernatant (b) was irradiated with a 532 nm green laser, the scattered green line was clearly observed in the liquid, suggesting the presence of a relatively large particle dispersion in the solvent. Therefore, we confirmed the original particle size distribution of Sample B in MeOH [Fig. 3(d)] by DLS measurement. The sizes were observed to be very narrowly distributed around 900 nm, indicating that the dispersed solution can maintain high transparency. The slightly larger particle size obtained by DLS measurement than that obtained by SEM observation is considered to be due to the absorption of organic solvent, causing the particles to swell.

Figure 4 shows the results of TG-DSC measurements performed to evaluate thermal durability. The crystal powder (Sample 1) showed an exothermic peak at 330–350 °C and a rapid decrease in thermogravimetry, indicating that it was undergoing combustion. Similarly, the spherical particles showed a slight weight loss due to the inclusion of MeOH solvent with a weak molecular interaction, but a rapid mass loss was observed at 320–330 °C. The spherical compound obtained had heat resistance to above 300 °C, although it was less heat resistant than the single crystals. An endothermic peak was observed at around 290 °C. This is the temperature at which the coordination bond between P=O and Eu breaks off, and we consider that the intrinsic structural stability of the first coordination sphere around Eu^{3+} is likely to be similar. Indeed, these spherical beads have high dispersibility in organic media, which has been a problem of previously prepared $[Eu(hfa)_3dpbp]_n$ polymers.

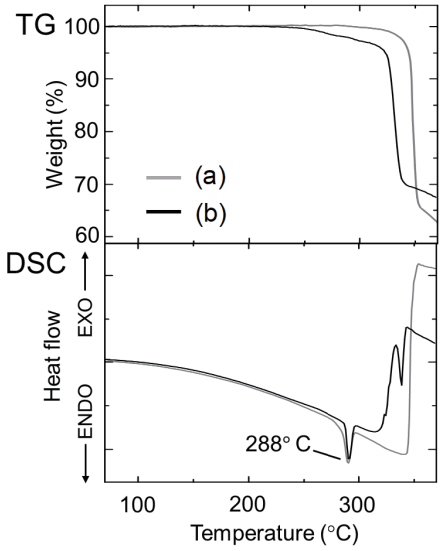

Fig. 4. TGA curves of $[Eu(hfa)_3dpbp]_n$: (a) Sample 1 and (b) Sample 2 in a nitrogen atmosphere at a heating rate of 10.0 °C/min.

3.2 Photophysical properties of different forms of $[Eu(hfa)_3dpdp]_n$ polymer

To discuss the difference in optical properties, Fig. 5(A) shows PL spectra of Eu^{3+} and Fig. 5(B) shows the decay curves of (a) the powder composed of block-shaped particles and (b) the spherical powder obtained by nanofiltration. In the PL spectrum in the range of 550–700 nm, five characteristic sharp peaks attributed to $^5D_0 \rightarrow {}^7F_J$, J = 0, 1, 2, 3, 4 due to the spin-orbit coupling of Eu^{3+} were observed. On the other hand, a comparison of the emission spectra reveals a clear difference in the spectral shape of the hypersensitive transition J = 2, suggesting that the coordination structure around Eu^{3+} is clearly different between Samples 1 and 2. This difference in the coordination structure around Eu^{3+} may be related to the difference around 20° observed by XRD. In addition, a J = 0–0 emission was induced at 578 nm in Sample 2, indicating that the coordination structure changed to the C_n symmetry.[10] Figure 5(B) shows the decay curves of $[Eu(hfa)_3dpbp]_n$ for (a) Sample 1, (b) Sample 2 in the solid state, and (c) Sample 2 in MeOH (1.0×10^{-4} M). The luminescence decay curve exhibits a linear slope on a logarithmic scale, suggesting single-component luminescence. The emission decay profiles of $[Eu(hfa)_3dpbp]_n$ are also shown in Fig. 5. The results and calculated photophysical values are listed in Table 1. The calculation details are given in the table caption. The lifetimes (τ_{obs}) of the spherical particles (solid state) and powder crystals were estimated to be 0.78 and 0.68 ms, respectively. The 4*f*–4*f* emission quantum yields (Φ_{Ln}) of the nanosize crystalline spheres and microsize solid-state crystals were calculated to be 79 and 69%, respectively. From the lifetime analysis results, it was found that the internal quantum efficiency and essential radiative lifetime τ_{rad} of the spherical particles without the solvent increased by nearly 10%. This is due to the difference in the Eu^{3+} coordination geometry. The nanosize bead LCPCs (Sample 2) have the same long-periodic structure (crystallinity) as the crystals of $[Eu(hfa)_3dpdp]_n$ (Sample 1), but the geometry around

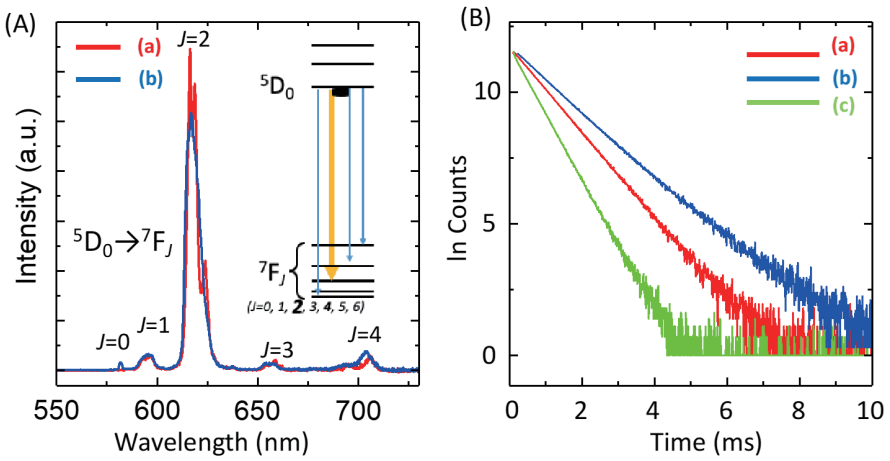

Fig. 5. (Color online) (A) PL and PLE spectra of $[Eu(hfa)_3dpbp]_n$: (a) Sample 1 and (b) Sample 2 in solid state. (B) Decay lifetime of $[Eu(hfa)_3dpbp]_n$: (a) Sample 1, (b) Sample 2 in solid state, and (c) Sample 2 in MeOH (1.0×10^{-4} M).

Table 1
Photophysical properties of $[Eu(hfa)_3dpbp]_n$: (a) Sample 1, (b) Sample 2 in solid state, and (c) Sample 2 in MeOH (1.0×10^{-4} M).

Sample	τ_{obs} (ms)	τ_{rad} (ms)*1	Φ_{Ln} (%)*1	k_r (s^{-1})	k_{nr} (s^{-1})
(a)	0.68	0.89	69	1100	510
(b)	0.78	0.99	79	1000	270
(c)	0.57	0.95	34	590	1200

*Values calculated by Werts equations.[11] Refractive index n ~1.5 in solid state and n ~1.33 in MeOH. Observed lifetimes (τ_{obs}) were measured. Radiative lifetime $\tau_{rad} = 1/_{AMD,0}\, n^3\, (I_{tot}/I_{MD})$, where $_{AMD,0}$ is the spontaneous emission probability for the $^5D_0$–$^7F_1$ transition in vacuo (14.65 s^{-1}), n is the refractive index of the medium (average refractive index of 1 employed for solid state), and (I_{tot}/I_{MD}) is the ratio of the total area of the corrected Eu emission spectrum to the area of the $^5D_0$–$^7F_1$ band. 4*f*–4*f* emission quantum yield $\Phi_{Ln} = \tau_{obs}/\tau_{rad}$. Radiative rate constant $k_r = 1/\tau_{rad}$. Nonradiative rate constant $k_{nr} = 1/\tau_{obs} - k_r$.

the lanthanides is different. On the other hand, when the spherical particles of Sample 2 were redispersed in methanol, the quantum efficiency showed a significant drop from 79 to 39%. This is due to the change in the vibrational structure owing to the intrusion of MeOH into the coordination crystals, as expected from the swelling of the particles. It is concluded that nanosize beads with excellent optical properties were obtained while maintaining high thermal stability.

3.3 Formation mechanism of different forms in crystalline $[Eu(hfa)_3dpdp]_n$ polymers

Finally, the formation mechanism of the spherical particles is discussed using the schematic diagram shown in Fig. 6. The illustration shows the two morphogenesis pathways of block and sphere formation using coordination and stacking equilibria in LCPCs.[12] The crystal growth of LCPCs proceeds by the rate balance of (1) coordination equilibrium reactions between lanthanides and organic ligands and (2) stacking equilibrium reactions due to intermolecular

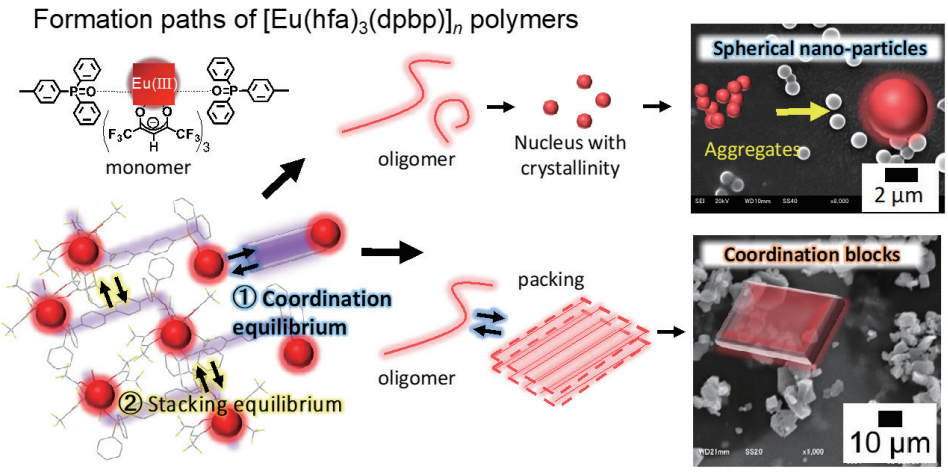

Fig. 6. (Color online) Two morphogenesis pathways, for blocks and spheres, using coordination and stacking equilibria in LCPC formation.

interactions. When the lanthanide salts (Eu^{3+}) and the coordinative bridging ligand (i.e., dpbp) are mixed, a rapid coordination equilibrium reaction begins and crystalline polymer chains with a length of several nanometers are formed. The polymer chains crystallize and form periodic structures through stacking reactions with adjacent molecules due to strong intermolecular forces. If the solute concentration is low, since the surface energy of polymeric crystals with a molecular size of several nanometers is unstable, they aggregate to minimize the energy. Indeed, the nanocrystals act as nuclei, and repeated aggregation between particles leads to nanosize spheres.

4. Conclusions

We successfully demonstrated the morphology control of spherical europium coordination polymer crystals $[Eu(hfa)_3dpbp]_n$ with thermal stability. The obtained spherical particles of size around 600–800 nm were well dispersed in MeOH and exhibited high emission quantum efficiency in the solid state. Spherical europium coordination beads are expected to be used in optical applications such as transparent full-color phosphor materials.

Acknowledgments

This research was financially supported by the Sensor and Actuator R&D Project of the National Institute for Materials Science. This work was also supported by Grants-in-Aid (Grant Numbers 17H04873 and 21H02031).

References

1 I. V. Taydakov, A. A. Akkuzina, R. I. Avetisov, A. V. Khomyakov, R. R. Saifutyarov, and I. C. Avetissov: J. Lumin. **177** (2016) 31.
2 V. V. Utochnikova, A. Grishko, A. Vashchenko, A. Goloveshkin, A. Averin, and N. Kuzmina: Eur. J. Inrg. Chem. **48** (2017) 5635.
3 S. Marchionna, F. Meinardi, M. Acciarri, S. Binetti, A. Papagni, S. Pizzini, V. Malatesta, and R. Tubino: J. Lumin. **118** (2006) 325.
4 H. Kataoka, T. Kitano, T. Takizawa, Y. Hirai, T. Nakanishi, and Y. Hasegawa: J. Alloys Compd. **601** (2014) 293.
5 C. Camp, J. Pe´caut, and M. Mazzanti: J. Am. Chem. Soc. **135** (2013) 12101.
6 N. Wartenberg, O. Raccurt, E. Bourgeat-Lami, D. Imbert, and M. Mazzanti: Chem. Eur. J. **19** (2013) 3477.
7 D. Sykes, S. C. Parker, I. V. Sazanovich, A. Stephenson, J. A. Weinstein, and M. D. Ward: Inorg. Chem. **52** (2013) 10500.
8 A. Nakajima, T. Nakanishi, Y. Kitagawa, K. Fushimi, and Y. Hasegawa: Sens. Mater. **28** (2016) 845.
9 K. Miyata, Y. Konno, T. Nakanishi, A. kobayashi, M. Kato, T. Nakanishi, K. Fushimi, and Y. Hasegawa: Angew. Chem., Int. Ed. **52** (2013) 6413.
10 K. Binnemans: Coord. Chem. Rev. **295** (2015) 1.
11 M. H. V. Werts, R. T. F. Jukes, and J. Verhoeven: Phys. Chem. Chem. Phys. **4** (2002) 1542.
12 C. A. Mirkin: Chem. Soc. Rev. **38** (2009) 1218.